

## Upper Limits on Planet Occurrence around Ultracool Dwarfs with K2

SHEILA A. SAGEAR,<sup>1</sup> JULIE N. SKINNER,<sup>2</sup> AND PHILIP S. MUIRHEAD<sup>1,2</sup>

<sup>1</sup>*Department of Astronomy, Boston University, 725 Commonwealth Ave., Boston, MA 02215, USA*

<sup>2</sup>*Institute for Astrophysical Research, Boston University, 725 Commonwealth Ave., Boston, MA 02215, USA*

Submitted to AAS Journals

### ABSTRACT

The occurrence of planets orbiting ultracool dwarfs is poorly constrained. We present results from a Guest Observer program on NASA’s K2 spacecraft to search for transiting planets orbiting a sample of 827 ultracool dwarfs. Having found no transiting planets in our sample, we determined an upper limit on the occurrence of planets. We simulated planets orbiting our sample for a range of orbital periods and sizes. For the simulated planets that transit their host, we injected the transit light curve into the real K2 light curves, then attempted to recover the injected planets. For a given occurrence rate, we calculated the probability of seeing no planets, and use the results to place an upper limit on planet occurrence as a function of planet radius and orbital period. We find that short period, mini-Neptune- and Jupiter-sized planets are rare around ultracool dwarfs, consistent with results for early- and mid-type M dwarf stars. We constrain the occurrence rate  $\eta$  for planets between 0.5 and 10  $R_{\oplus}$  with orbital periods between 1 and 26.3 days.

**Keywords:** planets and satellites: detection — stars: brown dwarfs — stars: late-type — stars: low-mass

### 1. INTRODUCTION

Statistical results from NASA’s Kepler Mission suggest a rapid increase in short-period, rocky planet occurrence with decreasing stellar mass (e.g. Howard et al. 2012; Gaidos et al. 2014; Dressing & Charbonneau 2015; Mulders et al. 2015). Short-period, rocky planet occurrence appears highest for mid-M dwarf stars, which host 1.2 planets per star with orbital periods of less than 10 days (Hardegree-Ullman et al. 2019); however, the occurrence rate for even later type stars and brown dwarfs is poorly constrained. Extrapolating planet occurrence rates from early and mid-M type to late-type M and cooler dwarfs, or ultracool dwarfs, we expect that they host even more short-period rocky planets. The discovery of seven planets transiting the M8 star TRAPPIST-1 (Gillon et al. 2016; Gillon et al. 2017) reinforces this expectation. However, the intrinsic faintness of ultracool dwarfs has historically limited large, statistical investigations into their planet occurrence rates.

He et al. (2017) searched for transiting planets in the photometric timeseries of 44 brown dwarfs obtained for the Weather on other Worlds program (Metchev et al. 2015), which used NASA’s Spitzer Space Telescope to study variability in L and T dwarfs. Finding no new exoplanets, they determined the occurrence rate of planets with with orbital periods less than 1.28 days and radii between 0.75 and 3.25  $R_{\oplus}$  to be  $\eta < 67\%$ . Demory et al. (2016) searched for transiting planets around 189 late M dwarfs observed by K2 and found no new planets. They show that TRAPPIST-1-like planets are able to be recovered in 10% of their sample, but “inflated” TRAPPIST-1-like planets that resemble super-earths that may still be rocky (1.5-2.5  $R_{\oplus}$ ) yield a higher recovery rate of up to 70%.

Motivated by the lack of discoveries coupled with the expectation of short-period rocky planets, we executed a Guest Observer program on NASA’s K2 Mission to search for exoplanets transiting ultracool dwarfs. The K2 Mission repurposed the original *Kepler* spacecraft for continued operations using only two reaction wheels (Howell et al. 2014). Unlike the primary Kepler Mission, which observed a single 100-square-degree sector of the

sky for nearly four years, the K2 Mission observed multiple 100-square-degree sectors of the sky spread across the ecliptic, each for approximately 80 days at a time. The greater sky coverage provided the opportunity to search hundreds of relatively bright, nearby ultracool dwarfs for short-period transiting planets.

In this paper, we present results from our K2 Guest Observer program. We searched for transiting planets in our sample of ultracool dwarf light curves. Similar to previous work, we did not discover new transiting planets. However, we used the non-detections to analyze the planet detection efficiency of *Kepler* in this regime and place upper limits on planet occurrence as a function of planet radius and orbital period. We used transit injection and recovery simulations to ascertain the likelihood of our null result, as a function of planet radius, orbital period and planet occurrence.

In Section 2, we discuss the sample of K2 ultracool dwarfs. In Section 3, we outline the data reduction and search for transiting exoplanets. In Section 4, we detail techniques used for transit injection and recovery. In Section 5, we present our constraints on planet occurrence rate, and in Section 6 we conclude with a discussion of our findings.

## 2. THE SAMPLE

To identify ultracool dwarfs in the K2 fields, we first selected spectroscopically confirmed ultracool dwarfs later than spectral type M5 from the online repositories maintained by J. Gagné (Gagné 2016a,b), which compiled ultracool dwarfs listed in Mace (2014), the DwarfArchives.org catalog (Gelino et al. 2016), and Dupuy & Liu (2012). Second, we searched the BOSS (Baryon Oscillation Sky Survey) Ultracool Dwarf catalog (BUD; Schmidt et al. 2015), which contains 11,820 M7-L8 dwarfs characterized through spectroscopy. We also identified a small subset of objects through the photometric survey from Skrzypek et al. (2016), who used the cross-section of SDSS (Sloan Digital Sky Survey) and WISE (Wide-Field Infrared Survey Explorer) with UKIDSS (UKIRT Infrared Deep Sky Survey) to identify ultracool dwarfs. In addition, roughly 30 of the targets were identified using colors and proper motions from the cross-match of 2MASS and ALLWISE (Schneider et al. 2016). The seven targets observed as a part of Campaign 7 were selected from the catalogs of Kirkpatrick et al. (2014) and Luhman & Sheppard (2014). We used the python package *k2fov* to identify which objects were within the field of view in a particular K2 campaign. In total, we identified 827 late-type M dwarfs and early-type L dwarfs bright enough to be observed as a part of K2. The sample used in our analysis contains data

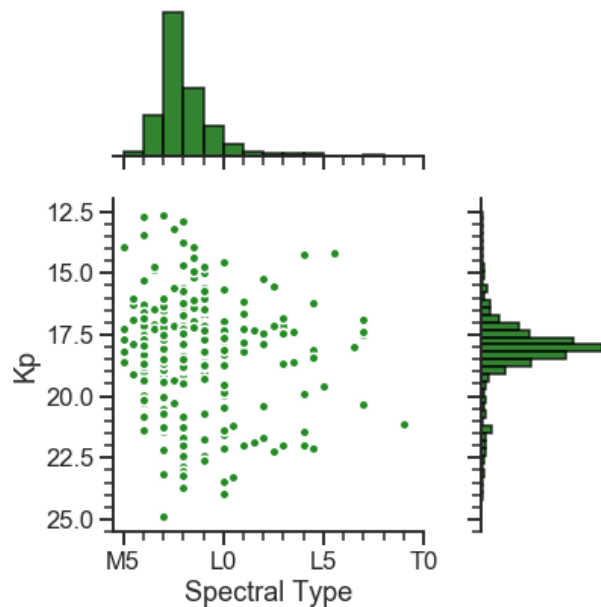


**Figure 1.** Spectral types and Kepler magnitudes for the 827 ultracool dwarfs in our sample. Most of the objects are mid-to-late M dwarfs, with  $\simeq 75$  L dwarfs.

from campaigns 5, 6, 7, 11, 12, 13, 14, 15, 16, 17, and 18. Of the 827 objects in our sample, 781 had spectral types derived from spectroscopy, primarily from the BUD catalog. For the remaining objects, we used spectral types assigned from photometry (Rodríguez et al. 2013). Figure 1 shows spectral types and Kepler magnitudes for the observed targets.

We provide the *Gaia* DR2 Source IDs for our sample (Gaia Collaboration et al. 2016, 2018). *Gaia* DR2 source IDs for 730 objects were obtained by performing a cross-match between our sample and the MLSDDS catalog (Kiman et al. 2019). The remaining objects were cross-matched with the full *Gaia* DR2 catalog using a 5" search radius. Proper motions and observation dates from SDSS were used to propagate coordinates to the *Gaia* DR2 epoch (2015.5) where available. A portion of the sample is shown in Table 1; the full version of Table 1 is available online.

## 3. DATA ANALYSIS AND PLANET SEARCH

We searched for planets around each of our 827 targets. For some targets, we searched for planets using more than one light curve if they were observed more than once in different campaigns. We searched a total of 1040 light curves.

We used K2 light curves reduced using the self flat-fielding method (SFF) developed by Vanderburg & Johnson (2014), which correlates flux variations with

**Table 1.** K2 Ultracool Dwarf Sample

EPIC ID	$\alpha$ (deg)	$\delta$ (deg)	Kp (mag)	Spectral Type	K2 Campaign	<i>Gaia</i> DR2 Source ID
248044306	67.53018	26.13911	16.41	M8.5	13	151296579553731456
248018652	67.73828	25.94430	15.90	M8	13	151102790629500288
247051861	68.06696	18.21287	12.69	M6	13	3314309890186259712
251456966	68.89929	21.25248	18.71	L0	13	
247581233	68.96430	22.81999	16.93	M8.5	13	145209339585095424
251456967	74.83841	15.68312	17.59	L0	13	3393271558253207680
246711015	75.55606	14.71022	15.63	L0	13	3392546632197477248
211936497	123.07013	19.27239	18.07	M7	18	669516407093922432
211783664	123.07365	17.08431	18.25	M7	18	656647826080870016
211541204	123.13754	13.71910	18.05	M7	18	650624465159332352

NOTE—The first 10 entries are shown here. The full version of this table with all 827 entries is available in the online version.

the pointing variations caused by K2’s spacecraft motion and removes the correlation. The flux values we use are taken from the aperture that provides the best photometric precision. The photometric precision is assessed by the the median value of a running standard deviation over bins of 13 observations, a similar metric to the Combined Differential Photometric Precision (CDPP), over a six-hour window (Vanderburg & Johnson 2014).

We downloaded the SFF-reduced light curves from the Mikulski Archive for Space Telescopes (MAST). The data described here may be obtained from the MAST archive. Due to the intrinsic faintness at optical wavelengths, many light curves show significant noise. Many objects also show evidence of rapid stellar rotation, which produces a periodic signal due to starspots rotating into and out of view, and stellar flares, which produce a sudden increase in brightness. A full analysis of the rotation and flaring activity for our sample is left as future work.

We normalized and sigma clipped the SFF-reduced light curves by discarding all points that fall farther than three sigma from the mean and replacing them with the mean value of all data points. We then detrended each light curve using a sliding window median filter with **untrendy**. This median filter creates a trend line from the median value of a sliding window of 10 points. We divided each normalized light curve by its trend line. We searched for transits in the processed light curves using the python implementation **python-bls**<sup>1</sup> of a box-

fitting least-squares (BLS) method (Kovács et al. 2002) to create a preliminary period and radius estimate. We searched for planets with periods from 1 to 28.57 days using 10,000 frequency bins and transit durations ranging from 0.1% to 30% of the total observation time.

Of the 827 targets in our sample, 248 were observed in multiple K2 campaigns. There were 211 targets observed in two campaigns and 35 targets observed in three campaigns. The same target was often observed multiple times in campaigns 5, 16, and 18, or campaigns 6 and 17. In order to increase the probability of detecting a planet, we stitched multiple observations together to create a longer light curve, preserving the timestamp of the observations. We searched these stitched light curves for planets in the same way as we search single campaign light curves.

We did not detect any transit signals around the 827 ultracool dwarfs that had a high enough confidence to be considered a threshold crossing event. The rest of this work focuses on the significance of this null result.

#### 4. INJECTION AND RECOVERY TESTS

To better understand K2’s sensitivity to planets around ultracool dwarfs, we simulated planets and attempted to recover them to measure the transit detection efficiency. We injected 10,000 randomly chosen synthetic planets into each of our 1040 K2 light curves and attempted to recover them, calculating the fraction of transits recovered in specific bins of period and radius. We used **ktransit** (Barclay 2015), a transit simulation package based on the Mandel & Agol (2002) limb-darkened transit model, to inject planets into the K2 light curves.

<sup>1</sup> <https://github.com/dfm/python-bls>

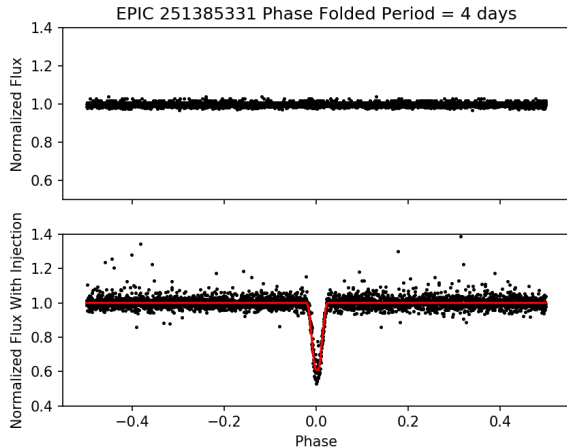


**Figure 2.** *Top:* The K2 light curve for EPIC 251385331, detrended and phase-folded over a period of four days. *Bottom:* The phase-folded and detrended light curve after injecting a synthetic planet with 0.6 stellar radii and period of four days. The red line shows the Levenberg-Marquardt fit.

To choose planet parameters to inject, we randomly drew a planet radius from a uniform distribution between 0.05 and 1.0 stellar radii. We randomly drew an inclination, assuming the orbital axis of each system may lie in any direction with equal likelihood. We allowed injections of planets with inclinations that do not produce a transit to account for the geometric transit probability when calculating an upper limit to planet occurrence. For this analysis, we considered only one transiting planet in the system.

As part of our detection criteria, we required that an injected planet transit at least three times. K2 observed a single patch of sky for approximately 80 days, so we only injected orbital periods between 1.0 and 26.3 days. We randomly chose a value within the orbital period limits from a logarithmic distribution. The final synthetic transit light curves we created have no noise or artifacts. We multiplied the synthetic transit light curves by the SFF-reduced K2 light curves, as shown in Figure 2.

We injected planets into the stitched, multi-campaign light curves the same way as we injected planets in single campaign light curves. When we stitched data from multiple campaigns together, we preserved the time stamps between subsequent observations so that when we injected a planet, the phase of the transit was in agreement with the observation time.

To recover our injected planets, we used the same BLS procedure we used in our original search for planets. We then refined our transit fit using the `ktransit` implementation of Levenberg-Marquardt minimization. We used the BLS period with the highest power, the square

root of the BLS transit depth, and an impact parameter of 0.0 as a starting point for the Levenberg-Marquardt fit.

For all objects with injected planets, we assumed a star with the same quadratic limb darkening model injected into all light curves. We considered a planet to be recovered if the recovered orbital period matches the injected orbital period within 5%, and if the recovered transit depth matches the injected transit depth within 25%. We searched for one transiting planet at a time in each light curve.

We assumed a stellar mass  $M_s$  of  $0.1M_\odot$  and a stellar radius  $R_s$  of  $0.1R_\odot$ , a reasonable estimation due to the narrow range of our sample’s spectral types (late-type M to L) and the corresponding narrow range of radii (Mann et al. 2015; Kesseli et al. 2019). We calculated an impact parameter  $b$  for each planet from an inclination  $i$  randomly chosen from a  $\sin(i)$  distribution using

$$b = \sqrt[3]{\frac{GMP^2}{(4\pi)^2} * \frac{\cos(i)}{R_s}} \quad (1)$$

If no part of the injected planet transits the star, or when the impact parameter is greater than

$$b = 1 + \frac{R_p}{R_s} \quad (2)$$

we did not carry on with a BLS search and transit fitting, and automatically marked the planet as unrecovered. This accounts for up to 90% of all injected planets.

For each planet injection and recovery, we recorded the injected orbital period, radius, and inclination, and whether the planet was successfully recovered.

The planet injection and recovery experiments show the threshold of detectability between planets that are generally recoverable and unrecoverable. Figure 3 shows this threshold for the K2 light curve of EPIC 229227260. We inject 50,000 random synthetic planets one by one into the light curve for this target, following the method above, and attempt to recover them. Planets between 0.15 and 0.25 stellar radii are recovered about 1% of the time depending on the orbital period and impact parameter. Smaller impact parameters (necessarily less than  $1 + \frac{R_p}{R_s}$ , as in Equation 2) and shorter orbital periods increase the likelihood of detectability. We are most sensitive to planets with orbital periods between 1.0 and 6.5 days and with radius  $0.15 \frac{R_p}{R_s}$  and larger, where 5% of injected planets were recovered around this star. For periods longer than 6.5 days, we recovered only 0.09% of injected planets around this star. The detectability threshold changes based on target brightness and signal-to-noise ratio of the light curve. The composite percent-

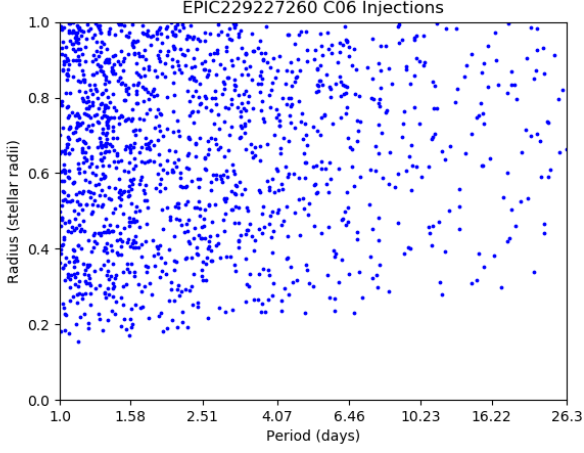


**Figure 3.** Injected and recovered planets around EPIC 229227260 in parameter space (orbital period vs. radius). 50,000 planets were injected with varying inclinations, about 5% of those planets transit the star, and 60% of those planets that transit are recovered. The division in parameter space between detectable and undetectable planets is apparent.

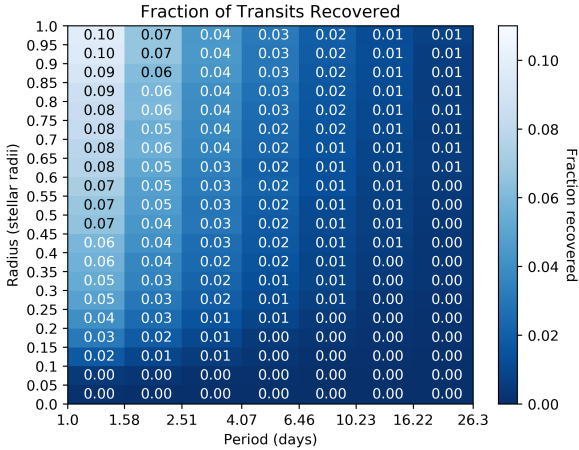


**Figure 4.** The fraction of planets we are able to detect after injecting 10,000 planets into each star in our sample. The detection efficiency is less than 0.1 for most bins because we vary the inclination for injected planets from 0 to 90 degrees, and most planets do not transit.

age of planets recovered, which we call the detection efficiency, is used to calculate the upper limit on planet occurrence. Figure 4 shows the fraction of transits we recover as a function of orbital period and  $\frac{R_p}{R_s}$ . For each bin of planet period and radius, we calculate the average detection efficiency, or percent of planets recovered, over 10,000 injections into the 827 K2 targets.

## 5. PLANET OCCURRENCE

We calculated the probability distribution of detecting no planets around  $n = 827$  ultracool dwarfs based on the detection efficiency and possible occurrence rates of planets. Each calculation is made for a planet within a specific orbital period and radius bin. Considering a specific orbital period and radius range, we multiplied the detection efficiency ( $d_i$ ) for this range by every possible planet occurrence rate (between 0 to 1). The probability of detecting no planets in a specific bin is shown in Equation 3.

$$P_{null} = \prod_{i=1}^n 1 - \eta * d_i \quad (3)$$

This product gives us the probability of not seeing a planet around an ultracool dwarf as a function of planet occurrence rate  $\eta$  from 0 to 1. We calculated  $P_{null}$  for every planet bin. The value of  $P_{null}$  defines the confidence level for the upper limit of  $\eta$ . The relationship between  $P_{null}$  and  $\eta$  can effectively be treated as a probability distribution of  $\eta$ .

We first set the probability of seeing zero planets around 827 ultracool dwarfs to less than 5%, and we calculated the upper limit of true planet occurrence  $\eta$  for each binned planet type. In Figure 5, a probability distribution of  $\eta$  for planets with orbital period between 1.0 and 1.58 days and radii from 0.95 to 1.0 stellar radii (the bin with highest detection efficiency), we determine that setting  $P_{null}$  to less than 5% yields an upper limit for  $\eta$  of 0.035. This means that no more than 3.5% of ultracool dwarfs host this type of planet. We calculated in a similar way the upper limit for  $\eta$  where  $P_{null}$  is less than 1% in Figure 6, which yields an upper limit for  $\eta$  of 0.053.

We calculated an upper limit for  $\eta$  in this way for each planet type according to the bins we used in Figure 4. Figure 7 shows the value of the upper limit of  $\eta$  for each planet type with  $P_{null} < 5\%$ . For planets that have a higher detection efficiency,  $\eta \simeq 0.1$  for short period (less than 4 days), large (greater than 0.2 stellar radii) planets. For planets we are not able to consistently detect, values of  $\eta$  range between 0.8 and 1 (i.e. planet occurrence is not well constrained in this regime). Figure 8 shows the upper limit on  $\eta$  for each planet type with  $P_{null} < 1\%$ .

## 6. DISCUSSION

We are more likely to detect short-period, large planets than long-period, small planets, as expected. The threshold for detectability is different for each target, but the smallest planets we are consistently able to recover are super-earths, which have an approximate  $\frac{R_p}{R_s}$  of 0.1 to 0.2.



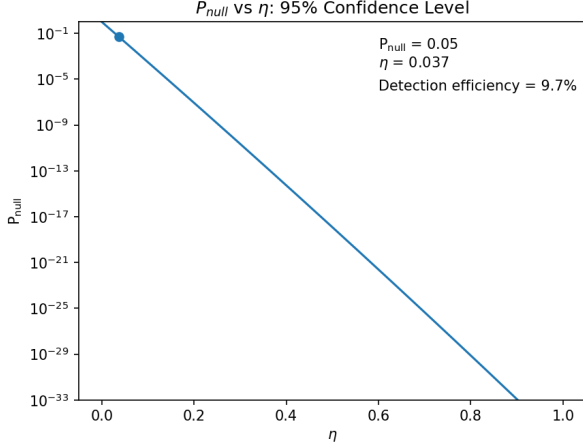


**Figure 5.**  $P_{\text{null}}$  is the probability of seeing no planets, as a function of true planet occurrence rate. This plot describes  $P_{\text{null}}$  for planets with periods between 1.0 to 1.58 days and  $R_p/R_s$  between 0.95 and 1.0, where  $P_{\text{null}} < 5\%$ .

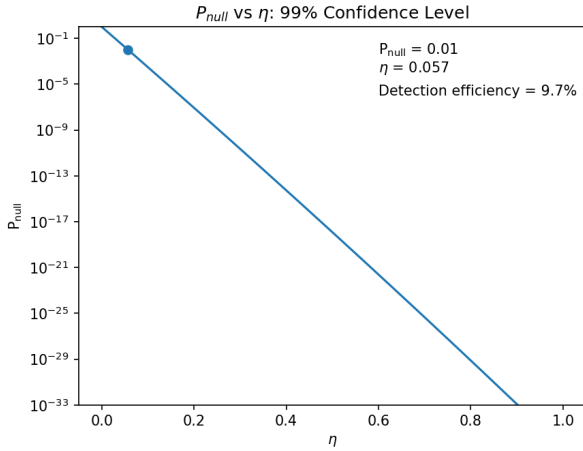


**Figure 6.** This plot describes  $P_{\text{null}}$  for planets with periods between 1.0 to 1.58 days and  $R_p/R_s$  between 0.95 and 1.0, where  $P_{\text{null}} < 1\%$ .

### 6.1. Planet Formation

Our results are consistent with constraints on planet formation in protoplanetary disks. [Rilinger et al. \(2019\)](#) measured the disk masses and radii of the protoplanetary disks around two brown dwarfs with spectral type M7. They found that one disk only contains enough material to form earth-mass planets and smaller, and one disk did not contain enough material to form planets at all. This implies that planets more massive than  $1 M_{\oplus}$  may be rare around brown dwarfs. [Payne & Lodato \(2007\)](#) also determined that for a brown dwarf with mass  $0.05 M_{\odot}$ , planet formation following the sequential core accretion model ([Pollack et al. 1996](#)) pro-

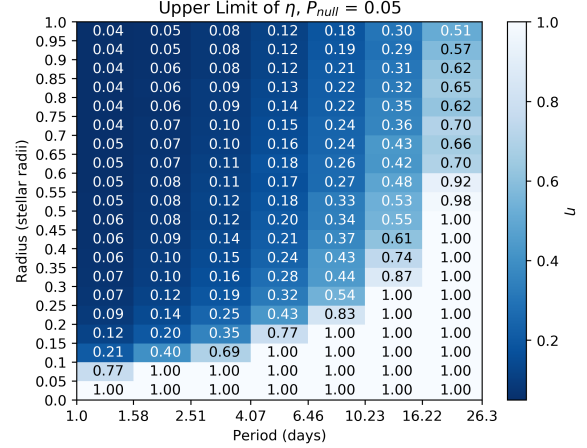


**Figure 7.** Upper limits on occurrence for each planet bin, with  $P_{\text{null}} < 5\%$ .

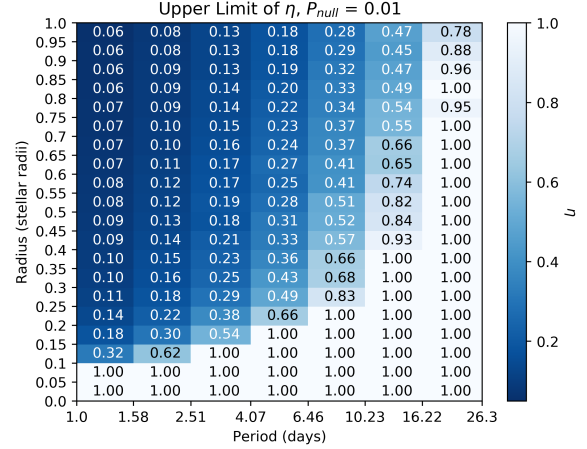


**Figure 8.** Upper limits on occurrence for each planet bin, with  $P_{\text{null}} < 1\%$ .

duces a maximum planetary mass of approximately  $5 M_{\oplus}$ . Our results are consistent with these findings, as the upper limit of  $\eta$  is most tightly constrained for hot mini-Neptunes and Jupiter-sized planets, suggesting that large planets are rare around ultracool dwarfs.

### 6.2. Comparison to [He et al. \(2017\)](#)

[He et al. \(2017\)](#) performed a planet search on a sample of 44 brown dwarfs (L3 to T8) observed by the Spitzer Space Telescope, which similarly returned a null result. They determined that the occurrence rate of planets around brown dwarfs with a period less than 1.28 days and a radius between 0.75 and 3.25 earth radii is  $\eta < 67\%$ .

For planets with periods less than 1.28 days and radii between 0.75 and 3.25 earth radii, they determined a

95% confident upper limit of  $\eta < 67 \pm 1\%$ . For periods less than 1.28 days and radii between 0.75 and 1.25 earth radii, they place a 95% confident upper limit of  $\eta < 87 \pm 3\%$ .

In similar bins, for planets with periods between 1 and 1.58 days and radii between 0.1 and .35 stellar radii, we find that when  $P_{null} < 5\%$  (equivalent to a 95% confidence) we place the upper limit of  $\eta$  between 21% and 7%, depending on the planet bins. When  $P_{null} < 1\%$ , we place the upper limit of  $\eta$  between 32% and 10%.

With a sample size of 827 ultracool dwarfs, we are able to place a tighter constraint on  $\eta$  than He et al. (2017). However, by utilizing data from Spitzer, they are able to include objects at later spectral types.

### 6.3. Comparison to Demory et al. (2016)

Demory et al. (2016) measured transit detection efficiency for “inflated” TRAPPIST-1b-like planets around mid- to late-M dwarfs, i.e. planets with short periods (less than three days) and up to 0.25 Jupiter radii (mini-Neptune sized). They determined that K2 is sensitive to close in mini-Neptunes, and they expect to recover 71% of these planets if they transit. However, their planet search yielded no detections. They determined that hot mini-Neptunes are rare around mid- to late-M dwarfs, as they are around early- to mid-M dwarfs (Dressing & Charbonneau 2015).

We also find that hot mini-Neptunes are rare around late-type M dwarfs and L dwarfs. For the hot mini-Neptunes we injected, planets with periods from 1 to 4.07 days and radius between 0.2 and 0.35  $R_s$ , we measured an average detection efficiency of 3.2% over all inclinations. Taking into account a transit probability of 5.4%, we expected to detect 60% of hot mini-Neptunes that transit, but we did not detect any of these planets. We place the upper limit of  $\eta$  for hot mini-Neptunes between 54% and 10%, suggesting that this type of planet is rare around ultracool dwarfs as well as M dwarfs at earlier spectral types.

## 7. SUMMARY

We searched for transiting planets in a sample of 827 ultracool dwarfs observed by K2 in long-cadence mode. The majority of our sample has spectral types between M6 to L5 determined from spectroscopy, with a handful of objects at later types. We found no transit events that met our detection criteria and thus use this

result to further investigate K2’s sensitivity to transiting planets around ultracool dwarfs

We performed injection and recovery tests and determined planet detection efficiencies for 827 ultracool dwarfs. The detection efficiencies were calculated using the BLS method and Levenberg-Marquardt optimization. Using these detection efficiencies, we determined upper limits on planet occurrence for planets between 0.05 and 1 stellar radii (about 0.5 to 10 earth radii) with periods between 1.0 and 26.3 days. We find that short period, gaseous planets are rare around ultracool dwarfs.

In the future, it will be useful to determine detection efficiency for multiple planets around ultracool dwarfs, since these objects have been previously shown to host groups of short-period planets in aligned systems: so-called compact multiples (Ballard & Johnson 2016).

This paper includes data collected by the K2 mission under Guest Observer Programs GO6037, GO7037, GO11022, GO12022, GO13022, GO14012, GO15012, GO16012, GO17025 and GO18025. Funding for the K2 mission is provided by the NASA Science Mission Directorate.

The authors acknowledge support from the NASA K2 Guest Observer Cycle 4 and K2 Guest Observer Cycle 5 programs under Grant Nos. NNX17AE91G and 80NSSC18K0294 issued through the Science Mission Directorate. The authors thank Aurora Kesseli for providing code to generate planet inclinations. The authors also thank Adam Schneider for useful conversations and for providing early access to the ALLWISE catalog of high proper motion objects.

S.S. acknowledges support from the Undergraduate Research Opportunities Program at Boston University and the Clare Boothe Luce Scholar Award.

All of the data presented in this paper were obtained from the Mikulski Archive for Space Telescopes (MAST). STScI is operated by the Association of Universities for Research in Astronomy, Inc., under NASA contract NAS5-26555. Support for MAST for non-HST data is provided by the NASA Office of Space Science via grant NNX13AC07G and by other grants and contracts.

### Facilities: K2

*Software:* `ktransit` (Barclay 2015); `python-bls`; `k2fov` (Mullally 2016); `astropy` (Astropy Collaboration et al. 2013; Price-Whelan et al. 2018); `Matplotlib` (Hunter 2007)

## REFERENCES

- Astropy Collaboration, Robitaille, T. P., Tollerud, E. J., et al. 2013, *A&A*, 558, A33, doi: [10.1051/0004-6361/201322068](https://doi.org/10.1051/0004-6361/201322068)
- Ballard, S., & Johnson, J. A. 2016, *The Astrophysical Journal*, 816, 66, doi: [10.3847/0004-637x/816/2/66](https://doi.org/10.3847/0004-637x/816/2/66)
- Barclay, T. 2015, *ktransit 0.2.2*, Zenodo, doi: [10.5281/zenodo.35265](https://doi.org/10.5281/zenodo.35265), <https://doi.org/10.5281/zenodo.15991>
- Demory, B.-O., Queloz, D., Alibert, Y., Gillen, E., & Gillon, M. 2016, *ApJL*, 825, L25, doi: [10.3847/2041-8205/825/2/L25](https://doi.org/10.3847/2041-8205/825/2/L25)
- Dressing, C. D., & Charbonneau, D. 2015, *ApJ*, 807, 45, doi: [10.1088/0004-637X/807/1/45](https://doi.org/10.1088/0004-637X/807/1/45)
- Dupuy, T. J., & Liu, M. C. 2012, *ApJS*, 201, 19, doi: [10.1088/0067-0049/201/2/19](https://doi.org/10.1088/0067-0049/201/2/19)
- Gagne, J. 2016a, List of All Ultracool Dwarfs. <https://jgagneastro.wordpress.com/list-of-ultracool-dwarfs/>
- . 2016b, List of M6-M9 Dwarfs. <https://jgagneastro.wordpress.com/list-of-m6-m9-dwarfs/>
- Gaia Collaboration, Prusti, T., de Bruijne, J. H. J., et al. 2016, *A&A*, 595, A1, doi: [10.1051/0004-6361/201629272](https://doi.org/10.1051/0004-6361/201629272)
- Gaia Collaboration, Brown, A. G. A., Vallenari, A., et al. 2018, *A&A*, 616, A1, doi: [10.1051/0004-6361/201833051](https://doi.org/10.1051/0004-6361/201833051)
- Gaidos, E., Mann, A. W., Lépine, S., et al. 2014, *MNRAS*, 443, 2561, doi: [10.1093/mnras/stu1313](https://doi.org/10.1093/mnras/stu1313)
- Gelino, C., Kirkpatrick, D., Cushing, M., Kinder, D., & Burgasser, A. 2016, *DwarfArchives.org*. <http://spider.ipac.caltech.edu/staff/davy/ARCHIVE/index.shtml>
- Gillon, M., Jehin, E., Lederer, S. M., et al. 2016, *Nature*, 533, 221, doi: [10.1038/nature17448](https://doi.org/10.1038/nature17448)
- Gillon, M., Triaud, A. H. M. J., Demory, B.-O., et al. 2017, *Nature*, 542, 456460, doi: [10.1038/nature21360](https://doi.org/10.1038/nature21360)
- Hardegree-Ullman, K. K., Cushing, M. C., Muirhead, P. S., & Christiansen, J. L. 2019, *AJ*, 158, 75, doi: [10.3847/1538-3881/ab21d2](https://doi.org/10.3847/1538-3881/ab21d2)
- He, M. Y., Triaud, A. H. M. J., & Gillon, M. 2017, *MNRAS*, 464, 2687, doi: [10.1093/mnras/stw2391](https://doi.org/10.1093/mnras/stw2391)
- Howard, A. W., Marcy, G. W., Bryson, S. T., et al. 2012, *ApJS*, 201, 15, doi: [10.1088/0067-0049/201/2/15](https://doi.org/10.1088/0067-0049/201/2/15)
- Howell, S. B., Sobeck, C., Haas, M., et al. 2014, *Publications of the Astronomical Society of the Pacific*, 126, 398, doi: [10.1086/676406](https://doi.org/10.1086/676406)
- Hunter, J. D. 2007, *Computing in Science & Engineering*, 9, 90, doi: [10.1109/MCSE.2007.55](https://doi.org/10.1109/MCSE.2007.55)
- Kesseli, A. Y., Kirkpatrick, J. D., Fajardo-Acosta, S. B., et al. 2019, *AJ*, 157, 63, doi: [10.3847/1538-3881/aae982](https://doi.org/10.3847/1538-3881/aae982)
- Kiman, R., Schmidt, S. J., Angus, R., et al. 2019, *AJ*, 157, 231, doi: [10.3847/1538-3881/ab1753](https://doi.org/10.3847/1538-3881/ab1753)
- Kirkpatrick, J. D., Schneider, A., Fajardo-Acosta, S., et al. 2014, *ApJ*, 783, 122, doi: [10.1088/0004-637X/783/2/122](https://doi.org/10.1088/0004-637X/783/2/122)
- Kovács, G., Zucker, S., & Mazeh, T. 2002, *A&A*, 391, 369, doi: [10.1051/0004-6361:20020802](https://doi.org/10.1051/0004-6361:20020802)
- Luhman, K. L., & Sheppard, S. S. 2014, *ApJ*, 787, 126, doi: [10.1088/0004-637X/787/2/126](https://doi.org/10.1088/0004-637X/787/2/126)
- Mace, G. N. 2014, PhD thesis, University of California, Los Angeles
- Mandel, K., & Agol, E. 2002, *ApJL*, 580, L171, doi: [10.1086/345520](https://doi.org/10.1086/345520)
- Mann, A. W., Feiden, G. A., Gaidos, E., Boyajian, T., & von Braun, K. 2015, *ApJ*, 804, 64, doi: [10.1088/0004-637X/804/1/64](https://doi.org/10.1088/0004-637X/804/1/64)
- Metchev, S. A., Heinze, A., Apai, D., et al. 2015, *ApJ*, 799, 154, doi: [10.1088/0004-637X/799/2/154](https://doi.org/10.1088/0004-637X/799/2/154)
- Mulders, G. D., Pascucci, I., & Apai, D. 2015, *ApJ*, 814, 130, doi: [10.1088/0004-637X/814/2/130](https://doi.org/10.1088/0004-637X/814/2/130)
- Mullally, Fergal; Barclay, T. B. G. 2016, *K2fov: Field of view software for NASA's K2 mission*, *Astrophysics Source Code Library*, doi: [10.5281/zenodo.44283](https://doi.org/10.5281/zenodo.44283), <http://dx.doi.org/10.5281/zenodo.44283>
- Payne, M. J., & Lodato, G. 2007, *MNRAS*, 381, 1597, doi: [10.1111/j.1365-2966.2007.12362.x](https://doi.org/10.1111/j.1365-2966.2007.12362.x)
- Pollack, J. B., Hubickyj, O., Bodenheimer, P., et al. 1996, *Icarus*, 124, 62, doi: <https://doi.org/10.1006/icar.1996.0190>
- Price-Whelan, A. M., Sipőcz, B. M., Günther, H. M., et al. 2018, *AJ*, 156, 123, doi: [10.3847/1538-3881/aabc4f](https://doi.org/10.3847/1538-3881/aabc4f)
- Rilinger, A. M., Espaillat, C. C., & Macías, E. 2019, *The Astrophysical Journal*, 878, 103, doi: [10.3847/1538-4357/ab211d](https://doi.org/10.3847/1538-4357/ab211d)
- Rodriguez, D. R., Zuckerman, B., Kastner, J. H., et al. 2013, *ApJ*, 774, 101, doi: [10.1088/0004-637X/774/2/101](https://doi.org/10.1088/0004-637X/774/2/101)
- Schmidt, S. J., Hawley, S. L., West, A. A., et al. 2015, *AJ*, 149, 158, doi: [10.1088/0004-6256/149/5/158](https://doi.org/10.1088/0004-6256/149/5/158)
- Schneider, A. C., Greco, J., Cushing, M. C., et al. 2016, *ApJ*, 817, 112, doi: [10.3847/0004-637X/817/2/112](https://doi.org/10.3847/0004-637X/817/2/112)
- Skrzypek, N., Warren, S. J., & Faherty, J. K. 2016, *ArXiv e-prints*. <https://arxiv.org/abs/1602.08582>
- Vanderburg, A., & Johnson, J. A. 2014, *PASP*, 126, 948, doi: [10.1086/678764](https://doi.org/10.1086/678764)